Journal of Power Sources 187 (2009) 544–554

Contents lists available at ScienceDirect

Journal of Power Sources

journal homepage: www.elsevier.com/locate/jpowsour

High pressure autothermal reforming in low oxygen environments

Mark A. Reese [1], Scott Q. Turn *, Hong Cui [2]

Hawaii Natural Energy Institute, University of Hawaii, 1680 East-West Rd., POST 109, Honolulu, HI 96822, United States

ARTICLE INFO

Article history:
Received 5 September 2008
Received in revised form 31 October 2008
Accepted 5 November 2008
Available online 21 November 2008

Keywords:
Methane
Autothermal reforming
Hydrogen peroxide
High pressure
Hydrogen production

ABSTRACT

Recent interest in fuel cells has led to the conceptual design of an ocean floor, fuel cell-based, power generating station fueled by methane from natural gas seeps or from the controlled decomposition of methane hydrates. Because the dissolved oxygen concentration in deep ocean water is too low to provide adequate supplies to a fuel processor and fuel cell, oxygen must be stored onboard the generating station. A lab scale catalytic autothermal reformer capable of operating at pressures of 6–50 bar was constructed and tested. The objective of the experimental program was to maximize H_2 production per mole of O_2 supplied ($H_{2(out)}/O_{2(in)}$). Optimization, using oxygen-to-carbon (O_2/C) and water-to-carbon (S/C) ratios as independent variables, was conducted at three pressures using bottled O_2. Surface response methodology was employed using a 2^2 factorial design. Optimal points were validated using H_2O_2 as both a stored oxidizer and steam source. The optimal experimental conditions for maximizing the moles of $H_{2(out)}/O_{2(in)}$ occurred at a S/C ratio of 3.00–3.35 and an O_2/C ratio of 0.44–0.48. When using H_2O_2 as the oxidizer, the moles of $H_{2(out)}/O_{2(in)}$ increased ≤14%. An equilibrium model was also used to compare experimental and theoretical results.

1. Introduction

The development of fuel cells and fuel cell powered vehicles has been a topic of great interest in recent years [1]. Fuel cells offer potential for higher efficiency and lower pollutant emissions when compared to traditional combustion-based power systems [2]. The proton exchange membrane fuel cell (PEMFC) is currently considered the most viable fuel cell technology for the near future [3–5]. As with almost all types of fuel cells, oxygen and hydrogen are supplied to a PEMFC in order to generate electrical power. Air, which is made up of ~21% oxygen, is most often used as the oxygen source [6]. Therefore, as long as the fuel cell operates in aerobic environments, a pump can provide a continuous air supply. Low oxygen environments however, encountered by sub-sea or space applications, pose the challenge of oxidant supply [7]. Additionally, hydrogen, while abundant, is not freely present in nature as molecular hydrogen and must be produced from another source such as water, hydrocarbons, or biomass. While it is likely that in the future, hydrogen will be produced by electrolysis using photovoltaic or wind power, currently the most economic way to produce hydrogen is by catalytic thermochemical reforming of hydrocarbons. Reforming technology has been a heavily researched topic and has been implemented in industry for some time.

In light of the current research and development of fuel cells and fuel processing techniques, there has been recent interest in constructing small scale, underwater, power generating stations. In concept, these remote units, using onboard fuel cells to generate power, would be deployed on the ocean floor where natural gas seeps or methane hydrates are present. Methane from these sources would be collected and purified to remove catalyst-poisoning H_2S. After purification the gas stream would be reformed to produce a hydrogen-rich gas for the fuel cell. While methane would be available in abundance, a major limitation for operating a reformer and fuel cell on the sea floor is having oxygen available at sufficiently high concentrations. Additionally, since the unit would be deployed on the ocean floor and operate at ambient pressure, design of components would need to accommodate the effects of elevated pressure on the physical system and reformer and fuel cell chemistry. An alternative to operating the reformer at ambient pressure would be to operate the reformer in a submerged pressure hull that would allow the system to operate at a lower pressure. The latter system would require that methane at the ambient pressure of the ocean floor be decompressed and that unwanted byproducts be recompressed for removal from the pressure hull. Operating the reformer at ambient pressure was selected over this alternative.

Applications include powering underwater sensory equipment and recharging unmanned submersibles. Currently, unmanned, untethered, vehicles (UUV) are predominately powered by batteries and therefore have a limited range. The mission range and duration

* Corresponding author. Tel.: +1 808 956 2346; fax: +1 808 956 2336.
E-mail addresses: mareese@hawaii.edu (M.A. Reese), sturn@hawaii.edu (S.Q. Turn), hongcui@hawaii.edu (H. Cui).
[1] Tel.: +1 808 956 2345; fax: +1 808 956 2344.
[2] Tel.: +1 956 5397; fax: +1 956 2344.

0378-7753/$ – see front matter © 2008 Elsevier B.V. All rights reserved.
doi:10.1016/j.jpowsour.2008.11.040

of battery powered UUV could be extended indefinitely if recharging could be completed underwater. It would also be beneficial if the vehicle did not have to surface in order to recharge, so as to avoid detection.

1.1. Fuel reforming

A fuel processor generally produces hydrogen from a hydrocarbon feedstock by one of three techniques: steam reforming (SR), partial oxidation reforming (POX), or autothermal reforming (ATR) [8,9]. SR and ATR reactors typically employ catalysts.

ATR combines thermal effects from both SR and POX reforming so that the heat required to support the endothermic steam reforming reaction is provided by oxidation reactions, resulting in a lower overall temperature [10]. ATR can be described by a reaction scheme based on the following four reactions:

Combustion of methane:

$$CH_4 + 2O_2 \rightarrow CO_2 + 2H_2O \quad (1)$$

Steam reforming reactions:

$$CH_4 + H_2O \leftrightarrow CO + 3H_2 \quad (2)$$

$$CH_4 + 2H_2O \leftrightarrow CO_2 + 4H_2 \quad (3)$$

Water gas shift (WGS):

$$CO + H_2O \leftrightarrow CO_2 + H_2 \quad (4)$$

By varying the reactant ratios of O_2 and H_2O with respect to the fuel, the set of reactions can be net endothermic, net exothermic, or thermally neutral. Also since ATR generates heat *in situ*, it does not require an external burner or heat exchangers like SR. When using methane as feedstock, Takeguchi et al. stated that while the equilibrium hydrogen production of ATR is slightly less than SR, the process consumes slightly more than half the heat [11]. ATR has been selected as the most promising reforming technique for the current application due to its simple design and efficiency for small scale systems.

1.2. Methane resource

The hydrocarbon feedstock for this specialized reforming application will come from two sources: marine natural gas seeps and methane hydrates. It has been estimated that 6–85 Tg of methane pass through the seabed of the continental shelves annually [12]. One of the most intense known seeps in the world, the Shane Seep (depth: 22–67 m), is located along the continental shelf just off shore from Santa Barbara, CA [13,14]. Other studied seeps include Coquille Bank located off shore from Cape Blanca, OR (depth: 132 m), Bluff Seep located off shore from Eel River, CA (depth: 43 m), and Hecta Bank Seep located off shore from Florence, OR (depth: 83 m) [15]. Analysis of gas samples from the Shane Seep taken over a period of several months showed a composition averaging 83.4% CH_4, 11.7% CO_2, 1.8% N_2, and 0.28% O_2, with the balance being classified as non-methane hydrocarbons [16]. These seeps provide a largely untapped supply of relatively pure methane that could be potentially harvested.

The second fuel source, methane hydrates, are ice-like crystalline structures with methane molecules held within the lattice of water molecules [17]. In 1999, Kvenvolden estimated the total global resource to be greater than 10^{15} m^3 but less than 10^{17} m^3 [18]. When appropriate expansion factors are applied, 1 m^3 of pure methane hydrate expands to approximately 164 m^3 of methane and 0.8 m^3 or water at standard pressure and temperature [19]. Methane hydrates thus provide an extremely dense source of methane which, after dissociation, could be collected in the gas phase at ambient pressures and used as a feedstock for reforming. Gas hydrates in the marine environment occur in the gas hydrate stability zone (GHSZ). The stability zone is dependent on temperature and pressure and, with favorable conditions, can begin at depths as shallow as 300 m below sea level [20].

1.3. Oxygen resource

Oxygen concentration in natural gas seeps and the dissolved oxygen concentration in sea water are very low. The highest recorded molar O_2 concentration in natural gas seeps in the literature reviewed was 0.3% [16] and the average molar O_2 concentration in sea water at depths where seeps are located is less than 0.0005% [21]. Given the low oxygen environment, oxygen storage will be required onboard the remote power unit to feed both the fuel reformer and the fuel cell.

One source of oxygen is the decomposition of hydrogen peroxide described by the following equation:

$$H_2O_{2(aq)} \rightarrow H_2O_{(aq)} + (1/2)O_{2(g)} \quad \Delta H = -98.1(\text{kJ mol}^{-1}) \quad (5)$$

The decomposition of hydrogen peroxide can thus provide O_2, H_2O, and heat, all of which could be utilized to operate a reformer and fuel cell on the seafloor. Moreover, since H_2O_2 is a liquid, the oxygen available per unit volume is high. This is desirable from the perspective of minimizing the size of storage tanks used to transport oxidizer from the surface to the seafloor. Pure H_2O_2 has a molarity of ~42 mol l^{-1} at 1 bar and 25 °C. Since the decomposition of 1 mole of H_2O_2 yields 0.5 mole of O_2, the oxidizer density is about 21 mol O_2 l^{-1} H_2O_2. In comparison, pure O_2 gas would have to be stored at 485 bar and 5 °C to attain a density of 21 mol l^{-1}. Additionally, H_2O_2 has a specific gravity of 1.4, which is double that of O_2 stored in the gas phase at 485 bar. This increase in density is beneficial as it provides negative buoyancy. Therefore, due to its favorable traits, H_2O_2 was selected as a candidate oxidizer for the system.

Purchasing H_2O_2 in a solution at a concentration greater than 50% by weight can be difficult and no effort was made to exceed this limit for safety reasons. H_2O_2 at 67% (weight) or greater can be dangerous as the heat of decomposition is sufficient to vaporize the water present in the solution and can lead to spontaneous decomposition. Therefore, while the heat of decomposition of high concentration H_2O_2 may lead to hazardous conditions, the heat of decomposition from lower concentration H_2O_2 solutions (<50% weight) is beneficial to the reforming process.

Hydrogen peroxide is common in the literature; often in papers dealing with propellants and very rarely in papers dealing with reforming. Patents [22] exist on the topic of using H_2O_2 for ATR reforming of methanol, ethanol, and other hydrocarbons. The basic concept in both patents is to decompose H_2O_2 to release steam, O_2, and heat to support ATR reactions. To date, outside of the patents, no papers have appeared which deal with the use of H_2O_2 as an oxidant for use in methane fuel reforming.

1.4. Objectives

The objective of this study was to determine optimal ATR operating conditions at 6, 28 and 50 bar and to conduct performance comparisons using H_2O_2 as both the steam and oxygen source. The range of selected pressures corresponds to operation at various natural gas seep depths as well as shallow methane hydrate formations. For this fuel-rich, oxygen limited, reforming application it is of particular interest to maximize moles of H_2 produced per mole of O_2 supplied.

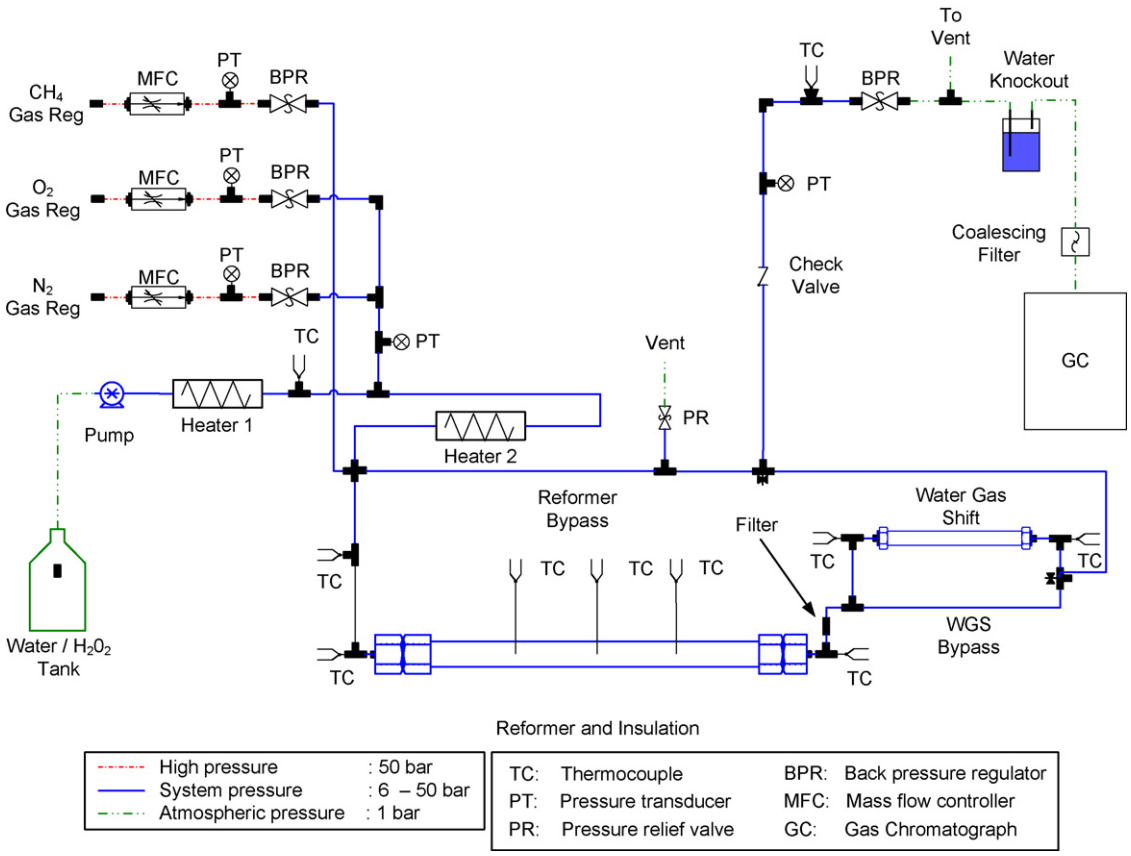

Fig. 1. Schematic layout of 50 bar reforming system.

2. Materials and methods

2.1. Experimental test facility

The schematic layout of the test facility is shown in Fig. 1. Methane (Grade 5.0), oxygen, and nitrogen from gas bottles were metered to the reactor using mass flow controllers (MFC) (Brooks 5850 Series E). Water or hydrogen peroxide solution was supplied to the reactor by a high pressure piston metering pump. Resistance element heat tracing was applied to the transfer lines between the reservoir and the reactor to pre-heat the liquid. Pressure in the reactor was set and controlled with a backpressure regulator. Flow rates were controlled and recorded along with temperatures and pressures using LabVIEW® (National Instruments, Austin, TX) running on a laptop computer. Temperatures of reactor inlet and outlet flows and three locations on the outside wall of the reactor were measured with thermocouples. To operate in autothermal mode, the reactor (61 cm long, XXS, 316 stainless steel pipe) was insulated with high temperature insulation (Thermcraft Inc., Winston-Salem, NC). To bring the reactor up to initial operating temperature, two spiral wound, resistance heating wire elements were inset in the insulation on either side of the reactor. Downstream of the reactor, the reformate passed through a condenser and coalescing filter (Balston, Model 31G) in series. The dry, effluent, gas was analyzed with a gas chromatograph (GC) (Shimadzu 14A, Columbia, MD) equipped with a Carboxen™ 1000 column (45/60, SUPELCO) and thermal conductivity detector (TCD).

2.2. Experimental design

A subsea power generating station located on the ocean floor would be operated at a fixed depth with an associated operating pressure. The focus of this study was to find optimal operating conditions at 6, 28, and 50 bar representing depths of 60, 280 and 500 m below sea level. In addition to pressure, other independent variables were the molar steam to carbon (S/C) and oxygen to carbon (O_2/C) ratios defined by the inlet flows of fuel, oxidizer, and water. Temperature and gas composition and yield were dependent variables.

Typically, parametric studies are used to observe the response of a dependent variable while each independent variable is incrementally changed over a specified range. For this study however, a 2^2 factorial design approach was used [23]. Utilizing surface response methodology (SRM), a two level factorial design allows both independent variables (S/C; O_2/C) to be changed simultaneously.

A sample of the 2^2 factorial design for this study is shown in Table 1. The first column "Order" refers to the randomized sequence of the experimental runs. Each "Run", generally comprised 5 or 6 gas samples and was conducted with the S/C and O_2/C ratios set to a high (+1) or low (−1) value as shown in columns 3 and 4. Using data from the literature [24], previous tests, and equilibrium calculations, the initial high and low values for both variables were selected as shown in Table 2. The fifth column in Table 1 refers to two level interactions of the two independent variables and is used later as an estimate of experimental error [23].

Table 1
Variable levels for factorial experimental design.

Order	Run	S/C	O_2/C	S/C × O_2/C interaction
2	1	−1	−1	1
4	2	1	−1	−1
3	3	−1	1	−1
1	4	1	1	1

Table 2
Initial operating conditions for low pressure (6 bar) experiments.

#	Variable name	Unit	Value		CH_4 flow l min^{-1}
			+	–	
1	S/C	/	3.75	2.25	2.50
2	O_2/C	/	0.58	0.46	2.50

The following is an overview of how the experimental design was conducted. After the initial factorial (4 runs) was completed, the results were analyzed to calculate the path of steepest ascent. This is the direction which caused the response variable to increase the greatest rate. New test conditions were then conducted along the path of steepest accent until a maximum response was found. Around this new found maximum, another factorial was conducted to confirm that the maximum had been found or to reveal a new path of steepest accent that would identify a new maximum.

2.3. Operating procedure

Standard operating procedures were followed each time an experiment was run. At the start of each new set of experiments (new pressure level), approximately 33 g of fresh, sulfide nickel catalyst on a gamma alumina support (Catalyst Ni-0309S, Engelhard, Newark, NJ) was loaded into the reactor. Under normal circumstances the same catalyst was generally left in the reformer for several days of testing. After the system integrity was verified by conducting a pressure test, calibration procedures were carried out for the GC and MFC's using certified standard gases and a bubble flow meter (mini-BUCK Calibrator M-30, A.P. BUCK, Orlando, FL), respectively.

After completing the calibration procedure the N_2 flow was set to 0.5 l min^{-1}, and the backpressure regulator on the system was turned to the open position. The reactor heating elements were energized until the catalyst bed rose above light off temperature. Typically the catalyst bed would reach about 650 °C in less than half an hour. At that temperature O_2 was metered into the reformer at the appropriate flow rate for the selected test and the CH_4 flow rate was set to 2.5 l min^{-1} (for all tests). Almost immediately a temperature increase in the reactor was detected due to the partial oxidation of CH_4. When the temperature increase was observed, the reactor heating element was turned off, the water pump and the water heating element were turned on, and the system pressure was set by adjusting the backpressure regulator. Within 45 min of turning on the water flow, the system temperatures and reformate gas composition were typically stabilized. The reformate gas was sampled every 10 min after temperatures and gas compositions stabilized. After several GC analyses were recorded for a given condition the S/C and O_2/C set points were changed and a new stable condition was generally acquired in 30 min or less. When the experimental run was completed, the CH_4 flow was turned off and the system was purged with O_2, N_2, and steam for several minutes

Table 4
Results of 2^2 factorial experiment showing the effect of changing S/C and O_2/C ratio one step on the $H_{2(out)}/O_{2(in)}$ yield.

Main effects	$H_{2(out)}/O_{2(in)}$	Error
S/C	0.037	±0.045
O_2/C	−0.102	±0.045
Interaction effect		
S/C × O_2/C	0.045	

2.4. Modeling

Thermochemical equilibrium conditions for reforming over a wide range of S/C and O_2/C ratios at 6, 28 and 50 bar were calculated using FACTSage™ 5.1 (Thermfact/CRCT, Montreal, Canada). The initial reactant gas species, reactant molar ratios, temperature, and pressure were specified for each run. Equilibrium results were calculated using final state points of system pressure and enthalpy equal to reactant conditions. The results served as a general comparative benchmark for experimental results.

3. Results and discussion

3.1. Methane reforming results at 6 bar pressure

Eighteen ATR runs were conducted at 6 bar using both bottled O_2 and liquid H_2O_2 solution as oxidizer. The results for all 6 bar tests are presented in Table 3 while Table 4 shows the individual effects of the S/C and O_2/C ratio on the molar ratio of $H_{2(out)}/O_{2(in)}$ for the first factorial. Table 4 also shows the two factor interaction effect, in this case the S/C and O_2/C ratios, which, according to Box et al. [23],

Table 3
Summary of autothermal reforming test results at 6 bar.

Run								Moles per mole of $CH_{4(in)}$								Total l min^{-1}
	S/C	O_2/C	Trials[a]	H_2/O_2	σ %	[H_2] %	σ %	H_2	σ %	CO	σ %	CH_4	σ %	CO_2	σ %	
1	3.00	0.52	6	4.06	0.6	68.75	0.1	2.12	0.5	0.20	0.4	0.19	0.9	0.61	0.4	8.25
2	2.25	0.58	8	3.83	2.5	69.79	1.0	2.23	3.3	0.31	8.0	0.11	9.0	0.58	5.2	8.53
3	3.75	0.58	6	3.99	0.4	70.70	0.1	2.33	0.2	0.20	1.3	0.12	0.8	0.68	0.2	8.77
4	3.75	0.46	6	4.10	0.5	66.05	0.1	1.90	0.4	0.11	1.4	0.29	0.7	0.60	0.2	7.67
5	2.25	0.46	5	4.12	0.8	65.65	1.9	1.90	1.0	0.18	5.7	0.27	1.5	0.55	1.6	7.70
6	3.35	0.44	5	4.14	1.1	64.86	1.9	1.84	1.4	0.12	24.4	0.29	8.2	0.56	3.0	7.50
7	3.50	0.40	BT[b]	4.08	0.0	62.66	0.4	1.63	1.8	0.08	4.8	0.37	0.7	0.52	3.2	6.93
8	3.00	0.52	4	4.07	1.6	68.40	0.7	2.07	1.4	0.19	0.6	0.18	0.7	0.60	0.8	8.08
9	3.00	0.52	5	3.88	0.7	66.95	1.8	2.01	0.4	0.27	1.3	0.19	1.2	0.51	0.6	7.96
10	3.35	0.44	3	3.98	0.5	64.40	0.1	1.74	0.8	0.09	1.2	0.33	0.5	0.55	0.8	7.27
11	2.60	0.48	4	3.99	1.0	66.48	0.4	1.90	1.1	0.16	1.9	0.26	2.2	0.55	1.2	7.67
12	4.10	0.48	BT[b]													
13	2.60	0.40	BT[b]	3.96	1.1	62.08	0.5	1.60	1.4	0.12	8.0	0.38	0.5	0.48	2.4	6.94
14	4.10	0.40	BT[b]													
15	3.35	0.44	3	4.02	0.5	64.57	0.1	1.76	1.1	0.10	1.5	0.33	0.5	0.55	0.9	7.32
16	3.35	0.44	6	3.95	0.6	64.54	0.3	1.75	0.8	0.09	1.9	0.33	0.8	0.55	0.3	7.30
17	3.35	0.44	5[c]	4.38	2.4	66.80	2.4	1.95	2.8	0.12	2.9	0.25	3.6	0.59	3.0	7.76
18	3.75	0.46	4[c]	4.47	1.6	68.29	0.3	2.04	1.6	0.11	3.1	0.23	2.8	0.63	1.7	8.03

[a] Trials are the number of repititions at each run condition.
[b] Indicates break through of high temperature reaction zone.
[c] Indicates H_2O_2 was used.

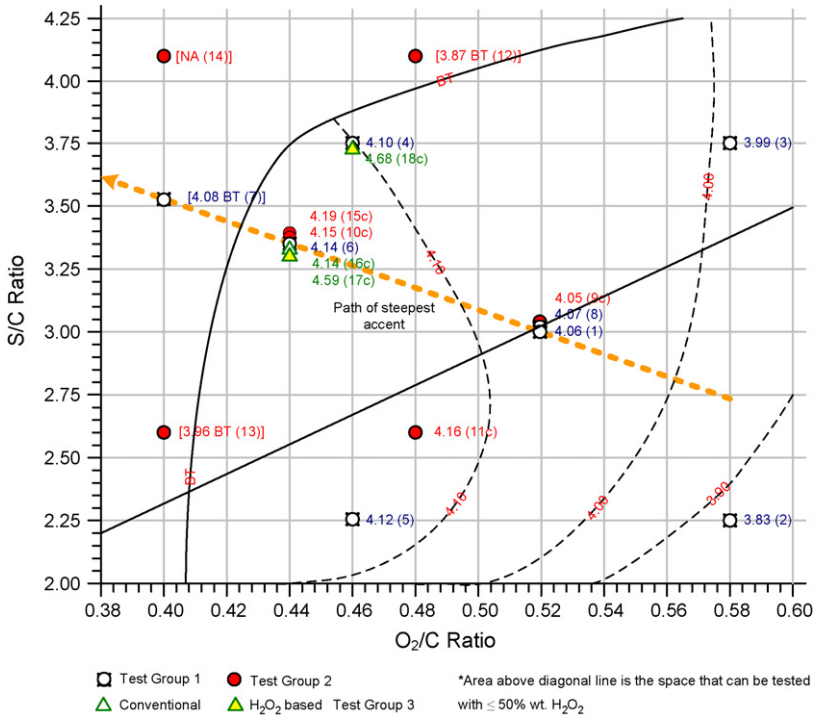

Fig. 2. Yield (moles H_2 per mole O_2) surface response of autothermal reforming as a function of S/C and O_2/C ratios based on corrected results at 6 bar operating pressure.

provides a reasonable approximation of variance and an estimate of experimental error.

Based on the initial factorial (runs #2 to #5), a path of steepest ascent was calculated to identify operating conditions that would increase the moles of $H_{2(out)}/O_{2(in)}$. The path is shown in Fig. 2 by a dashed line which passes through the center point of the first factorial. Two runs were completed along this path; run #6 produced a slight increase in yield while run #7 resulted in a yield decrease before the high temperature reaction zone blew out of the backend of the reformer. The center point, first factorial, and the path of steepest ascent (runs #1 to #8) made up test group 1. The first test point along the path of steepest ascent (S/C = 3.35 and an O_2/C = 0.44) was the test condition with the highest yield and was used as the center point for a second factorial.

Runs #9 to #15 made up test group 2 and were conducted 4 days after the first 8 runs were completed. These runs included replicating old conditions (for comparison) as well as running the second factorial. A correction factor of 4.25%, the average decrease in yield from replicated runs, was later used to correct all group 2 test results. The same catalyst was reused in test group 2 as was used in test group 1.

When attempting to run the second factorial it was only possible to attain steady-state operation for one of the four conditions. Run #12 and #13 were attempted but in both cases the high temperature reaction zone blew out of the backend of the reactor. This was due to the high S/C ratio in run #12 and the low O_2/C ratio in run #13. Run #14 was not attempted.

Finally, two performance comparisons using H_2O_2 as oxidizer were conducted, making up test group 3. Again to compensate for day to day differences, the results for test group 3 were multiplied by a correction factor of 4.8%, the percentage difference between run #6 and run #16: a run replicated from test groups 1 and 3, respectively.

Table 5
Summary of autothermal reforming test results at 28 bar.

Run								Moles per mole of $CH_{4(in)}$								Total l min^{-1}
	S/C	O_2/C	Trials[a]	H_2/O_2	σ %	[H_2] %	σ %	H_2	σ %	CO	σ %	CH_4	σ %	CO_2	σ %	
1	3.00	0.48	5	3.12	0.4	60.68	0.0	1.49	0.4	0.10	0.2	0.37	0.2	0.51	0.3	6.63
2	2.25	0.54	5	2.82	1.5	61.04	0.8	1.52	2.1	0.16	3.1	0.32	1.5	0.51	1.5	6.71
3	2.25	0.42	6	2.87	1.0	55.17	0.7	1.21	1.4	0.09	4.3	0.46	1.1	0.43	0.7	5.93
4	3.75	0.54	6	3.07	0.8	63.01	0.5	1.66	1.2	0.11	4.1	0.31	1.5	0.60	0.7	7.14
5	3.75	0.42	BT[b]													
6	2.25	0.54	5	2.63	3.4	58.86	2.1	1.42	4.8	0.16	7.5	0.36	4.6	0.49	1.6	6.49
7	3.00	0.48	5	3.47	0.2	62.45	0.1	1.67	0.2	0.13	2.0	0.36	0.6	0.54	0.3	7.26
8	3.00	0.48	6[c]	3.82	1.2	64.50	0.5	1.83	1.5	0.15	4.3	0.31	1.9	0.59	1.9	7.72
9	3.75	0.54	5	3.35	0.7	64.12	0.5	1.80	0.4	0.12	0.4	0.32	0.8	0.61	0.6	7.63
10	3.75	0.54	5[c]	3.52	0.9	64.90	0.2	1.89	1.0	0.14	0.9	0.28	1.2	0.64	1.2	7.90
11	3.75	0.42	BT[b]													
12	3.75	0.42	BT[b,c]													
13	3.00	0.54	4	3.38	0.7	65.44	0.3	1.82	0.7	0.14	0.8	0.27	2.0	0.59	0.3	7.50
14	3.00	0.48	3	3.39	1.0	62.37	0.5	1.62	1.3	0.11	2.6	0.35	1.0	0.54	0.6	6.99

[a] Trials are the number of repititions at each run condition.
[b] Indicates break through of high temperature reaction zone.
[c] Indicates H_2O_2 was used.

Table 6
Summary of autothermal reforming test results at 50 bar.

Run								Moles per mole of $CH_{4(in)}$								Total l min^{-1}
	S/C	O_2/C	Trials[a]	H_2/O_2	σ %	[H_2] %	σ %	H_2	σ %	CO	σ %	CH_4	σ %	CO_2	σ %	
1	3.00	0.48	5	2.75	1.0	56.67	0.0	1.31	0.4	0.08	1.0	0.43	2.2	0.50	0.8	6.24
2	3.75	0.54	5	2.77	1.2	60.05	0.9	1.49	2.2	0.09	3.3	0.36	2.2	0.56	1.1	6.70
3	2.25	0.54	4	2.21	0.9	54.48	0.6	1.19	0.6	0.10	4.9	0.41	3.1	0.48	1.2	5.90
4	2.25	0.42	3	1.89	4.0	44.70	3.6	0.80	5.4	0.06	7.7	0.53	3.3	0.37	2.0	4.85
5	3.75	0.42	BT[b]	2.73	1.5	53.84	0.9	1.15	2.0	0.06	22.9	0.47	1.8	0.45	1.6	5.78
6	3.00	0.47	4	2.93	1.5	58.94	1.4	1.38	1.4	0.09	1.7	0.39	5.4	0.50	0.9	6.43
7	3.68	0.49	6	2.81	0.6	58.41	0.3	1.36	0.7	0.08	1.2	0.39	0.4	0.51	0.3	6.40
8	3.75	0.53	5	2.71	0.7	59.69	0.2	1.43	0.9	0.09	1.2	0.35	0.6	0.54	0.8	6.56
9	3.00	0.48	4	2.87	0.7	58.43	0.3	1.38	0.9	0.08	0.9	0.40	0.6	0.50	0.9	6.44
10	3.00	0.48	4[c]	3.08	2.2	59.77	0.7	1.48	1.9	0.10	1.0	0.37	4.6	0.54	2.2	6.76
11	3.75	0.54	4	2.70	0.8	59.98	0.4	1.46	1.0	0.08	1.6	0.35	0.8	0.54	0.6	6.65
12	3.75	0.54	5[c]	2.94	0.8	62.02	0.2	1.59	0.9	0.11	0.7	0.30	0.6	0.58	0.8	6.99

[a] Trials are the number of repititions at each run condition.
[b] Indicates break through of high temperature reaction zone.
[c] Indicates H_2O_2 was used.

In Fig. 2 the type of data point marker used to depict the run conditions also shows test grouping. The number to the right of the marker is the moles of $H_{2(out)}/O_{2(in)}$ and the number in brackets following the yield is the run number as identified in Table 3. "BT" refers to conditions where the high temperature reaction zone blew through the backend of reactor. If a number is listed before the BT label, it refers to the yield before the high temperature reaction zone blew through. Estimated contour lines have been added to the figure to show the $H_{2(out)}/O_{2(in)}$ yield based on the experimental results. A "c" is used after the run number to indicate the results have been multiplied by a correction factor.

From Fig. 2 the optimum condition appears to be a broad plateau which is bounded on the left and at the top by a physical inability to stabilize the high temperature reaction zone in the reactor. Generally speaking the O_2/C ratio has a greater effect on the moles of $H_{2(out)}/O_{2(in)}$ than the S/C ratio.

3.2. Methane reforming results at 28 and 50 bar pressure

Fourteen ATR runs were conducted at 28 bar, and 12 runs were conducted at 50 bar using both bottled O_2 and H_2O_2 as oxidizer. The results are presented in Tables 5 and 6, respectively. Additional graphical summaries of test conditions run at 28 and 50 bar are shown in Figs. 3 and 4, respectively. Correction factors have again been added to account for day to day variance. The layout and symbols used are the same as those used in Fig. 2.

The optimum condition at 28 bar shifted to a higher O_2/C ratio compared to the 6 bar optimum, and therefore required additional O_2 input. Additionally, the maximum yield of $H_{2(out)}/O_{2(in)}$ decreased from approximately 4.16 moles to approximately 3.43 moles. This is a decrease of 17.5%. Since lower pressures favor the steam reforming reactions, a decrease in the $H_{2(out)}/O_{2(in)}$ yield was expected with increased pressure.

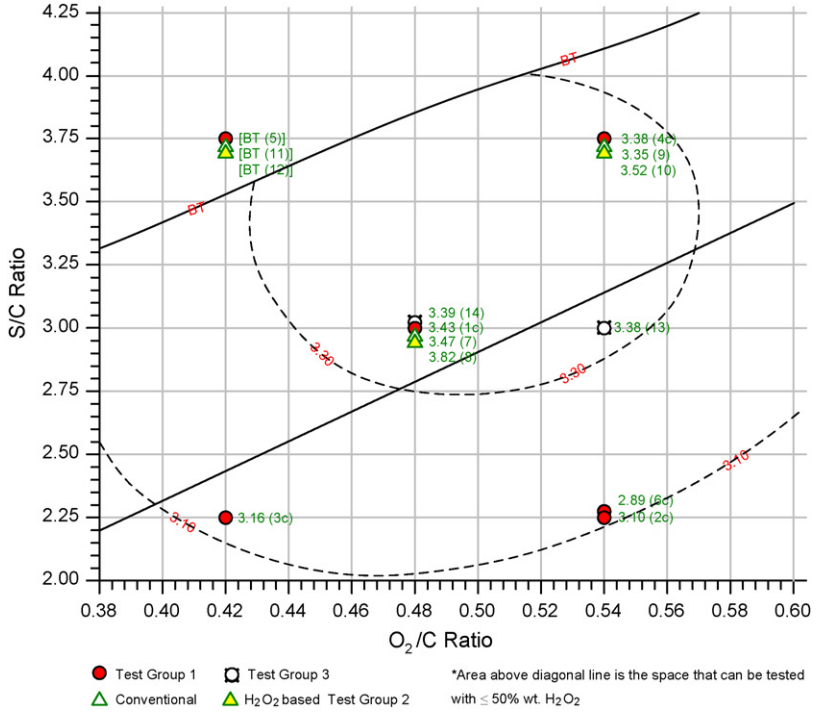

Fig. 3. Yield (moles H_2 per mole O_2) surface response of autothermal reforming as a function of S/C and O_2/C ratios based on corrected results at 28 bar operating pressure.

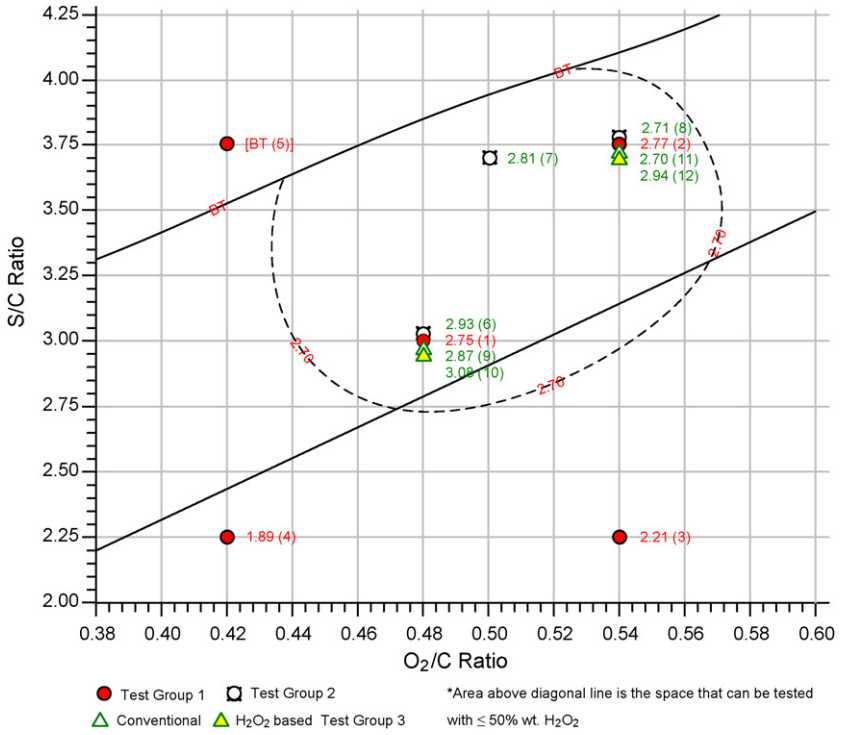

Fig. 4. Yield (moles H_2 per mole O_2) surface response of autothermal reforming as a function of S/C and O_2/C ratios based on corrected results at 50 bar operating pressure.

The optimum condition at 50 bar is in the same region as the optimum for 28 bar. The maximum yield of $H_{2(out)}/O_{2(in)}$ decreased from approximately 3.43 moles to approximately 2.87 moles. This is a decrease of 16.3%. Since lower pressures favor the steam reforming reactions, a decrease in the $H_{2(out)}/O_{2(in)}$ yield was expected with increased pressure.

3.3. Equilibrium model results

For comparison with experimental results, Figs. 5–7, show the H_2 yield (moles H_2 produced per mole of O_2 fed into the reactor) predicted by thermochemical equilibrium at 6, 28, and 50 bar, respectively. These results are based on ATR with O_2 as the oxidizer. The initial temperature of the reactants was set to 270 °C to match the pre-heated reactants delivered to the experimental reformer.

The white area at the upper left of the charts indicates a region where equilibrium does not predict H_2 in the products. This phenomenon was also observed experimentally although the exact location of the boundary of the region where H_2 is present in the products differs as explained later. The darker shaded areas indicate a broad plateau where H_2/O_2 ratios are high. The white area and the high yielding areas are separated by a steep gradient in $H_{2(out)}/O_{2(in)}$ productivity.

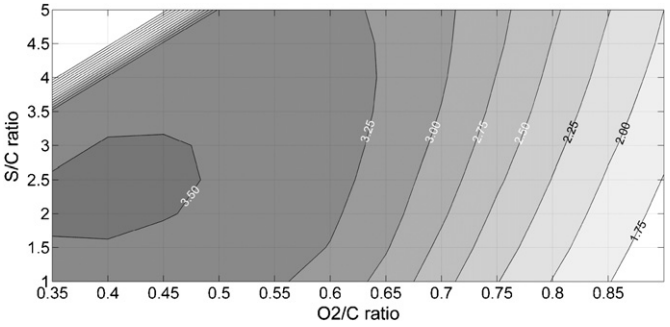

Fig. 6. Yield (moles H_2 per mole O_2) surface response of autothermal reforming as a function of S/C and O_2/C ratios based on thermochemical equilibrium results at 28 bar operating pressure and no system heat loss.

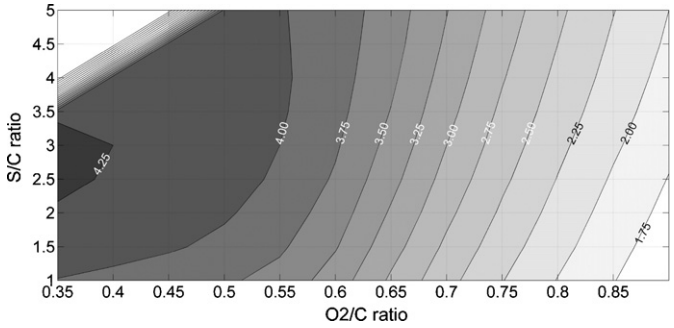

Fig. 5. Yield (moles H_2 per mole O_2) surface response of autothermal reforming as a function of S/C and O_2/C ratios based on thermochemical equilibrium results at 6 bar operating pressure and no system heat loss.

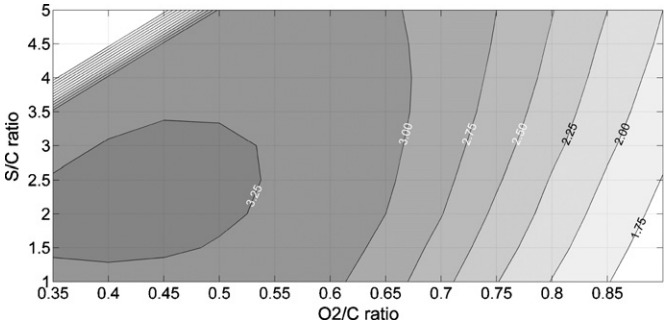

Fig. 7. Yield (moles H_2 per mole O_2) surface response of autothermal reforming as a function of S/C and O_2/C ratios based on thermochemical equilibrium results at 50 bar operating pressure and no system heat loss.

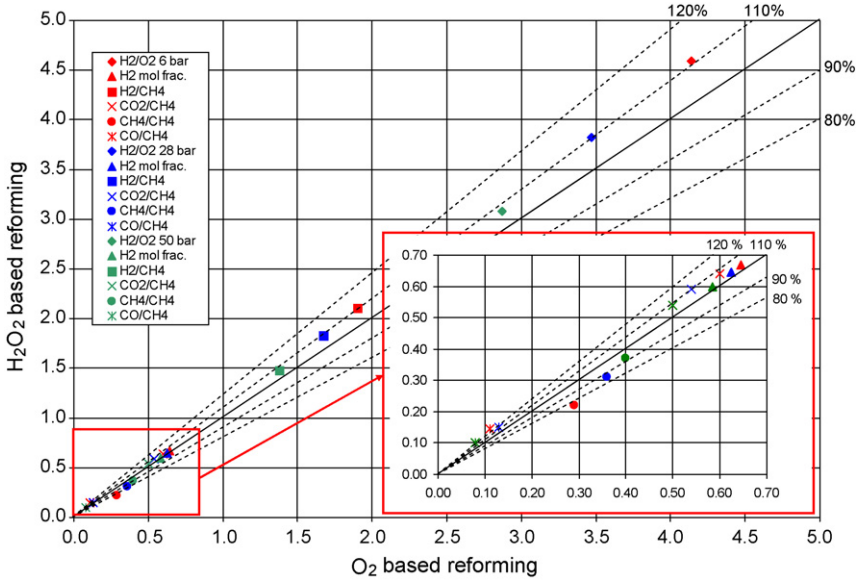

Fig. 8. Comparison of ATR experimental results from tests using O_2 and H_2O_2 as oxidizer/reactant at optimal conditions for 6 bar (red points), 28 bar (blue points), and 50 bar (green points). All ratios are (moles of product)/(mole of reactant) (Mol frac. = mole fraction). (For interpretation of the references to color in this figure legend, the reader is referred to the web version of the article.)

Comparing the equilibrium results at 6 bar (Fig. 5) to 28 bar (Fig. 7) the following observations were made: (1) the maximum $H_{2(out)}/O_{2(in)}$ value dropped 16% from 4.35 to 3.64, (2) the optimum condition changed from a S/C ratio of 3.00 and an O_2/C ratio of 0.35 at 6 bar to a lower S/C ratio of 2.5 and a higher O_2/C ratio of 0.4 at 28 bar, (3) both pressures exhibit a large plateau of insensitive $H_{2(out)}/O_{2(in)}$ yield in response to changes in the S/C and O_2/C operating parameters near the maximum value.

Comparing the equilibrium results at 28 bar (Fig. 6) to the results at 50 bar (Fig. 7) the following observations were made: (1) the maximum moles of $H_{2(out)}/O_{2(in)}$ dropped 8% from 3.64 to 3.36, (2) the optimum shifted slightly from S/C ratio of 2.5 and an O_2/C of 0.40 at 28 bar to the same S/C ratio with an increased O_2/C ratio of 0.45 at 50 bar, (3) the large plateau of insensitive $H_{2(out)}/O_{2(in)}$ yield in response to changes in the S/C and O_2/C operating parameters near the maximum is present at both pressures, (4) the $H_{2(out)}/O_{2(in)}$ results away from the optimum condition vary little with increased pressure.

3.4. Experimental results comparison: O_2- vs. H_2O_2-based ATR

Fig. 8 shows a parity plot comparing ATR results from experiments using O_2 and H_2O_2 as oxidizer at 6, 28, and 50 bar. Note that the results correspond to the optimal condition identified using O_2 as oxidizer. The H_2/O_2 in the legend refers to the moles of $H_{2(out)}/O_{2(in)}$ while the H_2/CH_4, CO_2/CH_4, CH_4/CH_4 and CO/CH_4 refer to moles of each species in the reformate per mole of $CH_{4(in)}$. Each pressure level shown is also color coordinated; red representing 6 bar, blue representing 28 bar, and green representing 50 bar.

When H_2O_2 was injected into the reformer as oxidizer, the moles of $H_{2(out)}$ and $CO_{2(out)}$ increased an average of 10%, the moles of $CO_{(out)}$ increased 10–25%, and the moles of $CH_{4(out)}$ decreased 9–25%. The mole fraction of H_2 in the reformate increased by 4% or less. Decomposition of H_2O_2 resulted in higher reactor temperatures which led to higher steam reforming rates but also pushed the water gas shift equilibrium slightly to the left (see Eq. (4)).

The decomposition of H_2O_2 began before it was injected into the reactor. An increased temperature in the reactant transfer lines and a reduced duty cycle of the controller for the heating elements on the reactant transfer lines served as indicators of the heat release from H_2O_2 decomposition reactions. Table 7 compares a set of test conditions conducted with O_2 (runs #16) and with H_2O_2 (run #17) at 6 bar. T_{in} and T_{out} are the temperatures at the inlet and outlet of the reactor catalyst bed, respectively. The heater duty cycle is the percentage of time that the pre-heater on the reactant transfer lines was energized. The heater output is calculated by multiplying the power consumed in the resistance wire heating element by the duty cycle of the heater.

The complete decomposition of H_2O_2 according to Eq. (5) would provide an additional input of 163 W of thermal energy to the system for run #17 compared to run #16. The decrease in pre-heater output, 614 W (run #16) to 529 W (run #17), accounts for 85 W. Using the gas flow rate, specific heats (c_p) of the gas components, and recorded temperatures, the change in the reactant temperature from 271 to 276 °C accounts for only 2 W. The increase in temperature of the outlet gas from 527 to 550 °C accounts for approximately 8 W. The flow rate of unconverted methane, $CH_{4(out)}$, was 0.20 l min^{-1} less in run #17 than in run #16. While several reac-

Table 7
Comparison of O_2- and H_2O_2-based ATR reforming.

Run	S/C	O_2/C	Trials[a]	T_{in} (°C)	T_{out} (°C)	Heater output (W)	Mol H_2/O_2	Mol $CH_{4(out)}$
16	3.35	0.44	6	271	527	54	4.14	0.83
17	3.35	0.44	4[b]	276	550	46	4.59	0.63

[a] Trials are the number of repitions at each run condition.
[b] Indicates H_2O_2 was used.

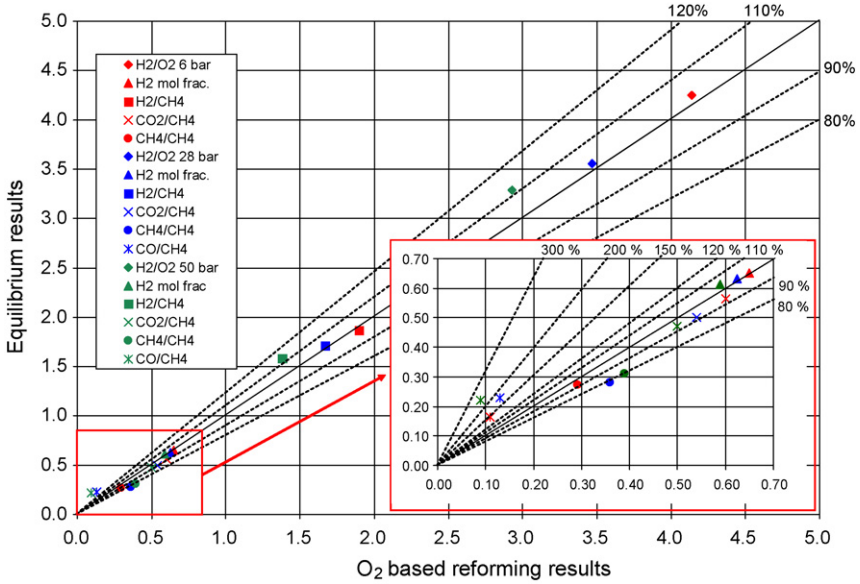

Fig. 9. Comparison of ATR experimental results from tests using O_2 as oxidizer/reactant and thermochemical equilibrium calculations at optimal conditions for 6, 28 and 50 bar.

tion pathways can account for this difference in CH_4 levels, the most likely explanation is an increase in endothermic steam reforming. The exothermic water gas shift reaction does not account for this difference in CH_4 concentration as the outlet temperature increased in run #17 and a temperature increase serves to reduce the WGS reaction. Therefore, based on the steam reforming equation shown in Eq. (2), approximately 30 W is calculated to be required to convert the 0.20 l min^{-1} CH_4.

Using this analysis, and summing up the 85 W + 2 W + 8 W + 30 W accounted for earlier and dividing by the total of 163 W provided by the decomposition of H_2O_2, 77% of the additional chemical energy entering the system as H_2O_2 can be accounted for. This leaves 23% or 38 W unaccounted for and this may be attributed to additional heat loss from the system.

3.5. Conventional experimental results vs. equilibrium calculations

Fig. 9 is a parity plot comparing equilibrium values with experimental ATR using O_2 as oxidizer at the optimal conditions for 6, 28 and 50 bar.

At 6 bar the predicted moles of $H_{2(out)}$ was only 3% greater than experimentally observed. The predicted moles of $CH_{4(out)}$, and $CO_{2(out)}$ differed by 7% or less from the experimental results. The moles of $CO_{(out)}$ however, were 49% greater. The equilibrium model predicted the temperature of product gas to be 640 °C compared to 512 °C for the experimental results. Overall the equilibrium model showed close agreement with the experimental results at 6 bar.

At 28 bar the predicted moles of $H_{2(out)}$ was again only 3% greater than the experimental yield. The predicted moles of $H_{2(out)}$ and $CO_{2(out)}$ were in close agreement with the experimental results, differing by 8% or less. The predicted moles of $CH_{4(out)}$ was 20% less than experimental while the moles of $CO_{(out)}$ was nearly 200% of the experimental value. The equilibrium model predicted the temperature of product gas to be 743 °C; 229 °C higher than recorded experimentally.

At 50 bar, as observed at lower pressures, the predicted moles of $H_{2(out)}$ and $CO_{2(out)}$ per mole of $CH_{4(in)}$ differed by 14% or less from experimentally observed. The predicted moles of $CH_{4(out)}$ was again 20% less than experimental, while the moles of $CO_{(out)}$ was 240% of the experimental value. The equilibrium model predicted the temperature of product gas to be 774 °C, 202 °C higher than was observed experimentally.

Differences between experimental and equilibrium results can be summarized as (1) observed moles of $H_{2(out)}$ were 97% of predicted values at 6 and 28 bar and 90% of the predicted value at 50 bar, (2) observed moles of $CH_{4(out)}$ were 105% of predicted value at 6 bar and 125% of the predicted value at 28 and 50 bar, (3) observed moles of $CO_{2(out)}$ were approximately 8% less than predicted over all pressures, (4) observed moles of $CO_{(out)}$ were 67–40% of equilibrium values and decreased with increasing pressure, and (5) the experimental outlet gas temperature was on average 186 °C lower than the temperature of products predicted by the equilibrium model. Disagreements indicate that the experimental results did not attain equilibrium and this may be due to non-idealities inherent in the experimental conditions, e.g. the equilibrium calculation does not include the effects of heat loss experienced by the experimental system.

To understand the differences, the temperature profile within the reactor can provide additional insight. The temperature profile in the reactor shown in Fig. 10 was captured by a thermocouple located in a stainless sheath at the backend of the catalyst bed as reaction zone slowly blew out of the reactor. As such, the maximum temperature shown would be lower than the maximum gas temperature and the peak shown would be significantly broader than the actual peak. Zone 1 primarily covers the heating of reactants from the oxidation of CH_4. Heating largely occurs by conduction through the catalyst bed from the very narrow high temperature region in Zone 2. Zone 2 is characterized by both oxidation and steam reforming reactions. By some point in Zone 2 all of the O_2 and approximately 25% of the CH_4 is consumed (O_2/C ratio ~0.5) according to Reaction (1). After the peak temperature is reached the steam reforming reactions (Reactions (2) and (3)) consume more heat than is produced and the temperature drops rapidly. This high temperature zone is relatively narrow and conversion in this zone may be limited by catalyst deactivation due to the high peak temperature. Deactivation of the catalyst in this region could be tolerated if the high temperature region is stabilized and provides the necessary heat to the surrounding, active catalyst bed. Further studies should be completed to determine if catalyst performance can be maintained for an extended duration at the observed peak temperatures.

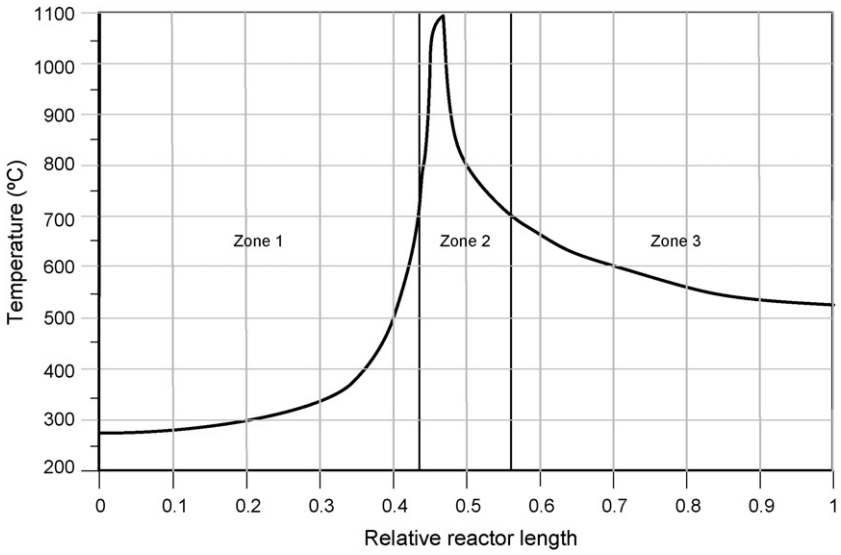

Fig. 10. Example experimental ATR temperature profile.

3.6. Comparison to relevant work

The most complete data set of experimental results in the literature was presented by Hoang et al. [24] and figures from this publication were analyzed to produce the comparative data shown in Fig. 11 for methane reforming at a pressure of 1 bar. Hoang et al. [24] stated that steam was introduced into the reactor but no further detail on reactant temperature was provided.

From Hoang's results, the maximum yield of $H_{2(out)}/O_{2(in)}$ was 3.0 and occurred at a S/C ratio = 1.8 and a O_2/C = 0.50. This is a marked difference from the present experimental and modeling results and it would appear that Hoang's reactant inlet temperature was significantly lower than the 270 °C inlet conditions in the present study. This would explain why the lower O_2/C and higher S/C ratios did not produce stable reaction conditions and also why the maximum value of $H_{2(out)}/O_{2(in)}$ yield occurred at a much higher O_2/C ratio. While the $H_{2(out)}/O_{2(in)}$ yield is significantly lower, the trends shown in Fig. 11 are very similar to the experimental results from the present study.

3.7. Different optimization criteria

Reforming experiments are often conducted to optimize the moles of $H_{2(out)}/CH_{4(in)}$. From the equilibrium calculations shown in Fig. 12, it is clear the optimum yield of $H_{2(out)}/CH_{4(in)}$ lies in a different region than the optimum yield for $H_{2(out)}/O_{2(in)}$. Within the limitations of the operating space, the optimum result is 2.36 moles of $H_{2(out)}/CH_{4(in)}$ at a S/C ratio = 5 and an O_2/C ratio = 0.65.

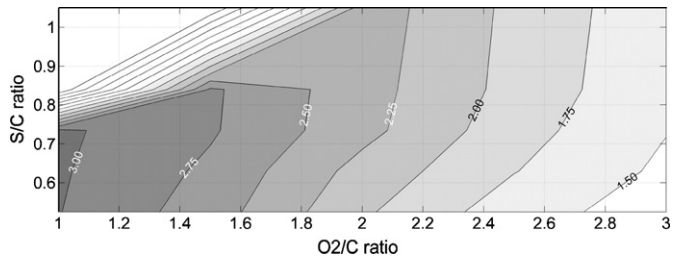

Fig. 11. Yield (moles H_2 per mole O_2) surface response of autothermal reforming as a function of S/C and O_2/C ratios based on results at 1 bar operating pressure from Hoang et al. [24].

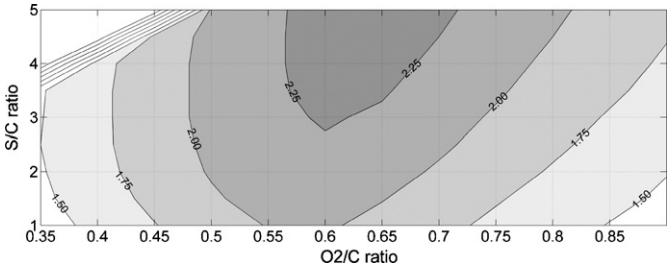

Fig. 12. Yield of moles of H_2 produced per mole of CH_4 fed into reactor (equilibrium values, 6 bar, no heat loss).

4. Conclusions

A lab scale experimental facility for catalytic autothermal reforming at pressures ranging from 6 to 50 bar was constructed and tested. This pressure range was selected as a design criterion for simulating conditions typical of the sea floor where natural gas seeps or methane hydrates are present. This environment presents unique fuel reforming operating conditions in that fuel is plentiful, oxygen is a limiting resource, and maximizing the hydrogen yield, i.e. moles of $H_{2(out)}/O_{2(in)}$, is of primary importance. From the tests it was noted that the optimum condition for maximizing the moles of $H_{2(out)}/O_{2(in)}$ was significantly different then maximizing the moles of $H_{2(out)}/CH_{4(in)}$ which is a more typical goal. The results of this study located optimum conditions for fuel reforming at pressures of 6, 28, and 50 bar. Employing data from experimental results and an equilibrium model, O_2-based reformer performance in response to changes in reactant ratios (S/C and O_2/C) was presented. Experimentally, the optimal conditions for maximizing the yield of $H_{2(out)}/O_{2(in)}$ occurred at a S/C ratio of 3.35 and an O_2/C ratio of 0.44 at 6 bar, a S/C ratio of 3.00 and an O_2/C ratio of 0.48 at 28 bar, and a S/C ratio of 3.00 and an O_2/C ratio of 0.48 at 50 bar. Under these conditions 1 mole of O_2 produced 4.16 moles of H_2 at 6 bar, 3.43 moles of H_2 at 28 bar, and 2.84 moles of H_2 at 50 bar. Proof of concept using H_2O_2 as a steam and oxidizer source was also validated. A minimum of two conditions were rerun using H_2O_2 at each of the three test pressures. An increase in $H_{2(out)}/O_{2(in)}$ yield of up to 14% was observed when H_2O_2 was used compared to results from bottled O_2-based ATR. A higher yield may have been achieved had there been a way to keep the H_2O_2 from partially decomposing before entering the reactor. This study is useful for identifying

optimal conditions for operating an ATR reformer in a high pressure, low oxygen environment where O_2 needs to be conserved, specifically subsea conditions. Additionally the use of H_2O_2 as an oxidizer for ATR is novel and may be of interest for other low oxygen environments such as space applications.

References

[1] R.J. Farrauto, Appl. Catal. B: Environ. 56 (1–2) (2005) 3–7.
[2] J. Larmine, A. Dicks, Fuel Cell Systems Explained, 2nd ed., 2005.
[3] A. Ersoz, H. Olgun, S. Ozdogan, J. Power Sources 154 (1) (2006) 67–73.
[4] S.H. Chan, D.L. Hoang, O.L. Ding, Int. J.Heat Mass Transf. 48 (19–20) (2005) 4205–4214.
[5] S. Ahmed, M. Krumpelt, Int. J. Hydrogen Energy 26 (4) (2001) 291–301.
[6] Z. Xu, Z. Qi, A. Kaufman, J. Power Sources 115 (1) (2003) 40–43.
[7] N.A. Choudhury, et al., J. Power Sources 143 (1–2) (2005) 1–8.
[8] M. Lyubovsky, D. Walsh, J. Power Sources 157 (1) (2006) 430–437.
[9] A. Faur Ghenciu, Curr. Opin. Solid State Mater. Sci. 6 (5) (2002) 389–399.
[10] S.H. Chan, H.M. Wang, Int. J. Hydrogen Energy 25 (5) (2000) 441–449.
[11] T. Takeguchi, et al., Appl. Catal. A: Gen. 240 (1-2) (2003) 223–233.
[12] M. Hovland, A.G. Judd, R.A. Burke Jr., Chemosphere 26 (1–4) (1993) 559–578.
[13] J.S. Hornafius, D. Quigley, B.P. Luyendyk, J. Geophys. Res. [Oceans] 104 (C9) (1999) 20703–20711.
[14] J.F. Clark, et al., J. Geophys. Res. [Oceans] 105 (C5) (2000) 11509–11522.
[15] R.W. Collier, M.D. Lilley, Geophys. Res. Lett 32 (6) (2005), pp. L06609/1–L06609/4.
[16] J.F. Clark, et al., Geo-Marine Lett. 23 (3–4) (2003) 187–193.
[17] A.V. Milkov, R. Sassen, Marine Geol. 179 (1–2) (2001) 71–83.
[18] K.A. Kvenvolden, Proc. Natl. Acad. Sci. U.S.A. 96 (7) (1999) 3420–3426.
[19] K.A. Kvenvolden, G.D. Ginsburg, V.A. Soloviev, Geo-Marine Lett. 13 (1) (1993) 32–40.
[20] W. Dillon, K.A. Kvenvolden, Gas (Methane) Hydrates—A New Frontier, U.S. Geological Survey Marine and Coastal Geology Program, 1992.
[21] Hawaii Ocean Time-series Data Organization & Graphical System, http://hahana.soest.hawaii.edu/hot/hot-dogs/interface.html.
[22] T. Xiao, Catalytic reaction between methanol and hydrogen peroxide to produce hydrogen, PCT Int. Appl., Isis Innovation Limited, UK, Wo, 2005, 24 pp.
[23] G.E.P. Box, W.G. Hunter, J.S. Hunter, Statistic for Experimenters, 1st ed., John Wiley and Sons, 1978, pp. 653.
[24] D.L. Hoang, S.H. Chan, O.L. Ding, J. Power Sources 159 (2) (2006) 1248–1257.